A comparison of uniaxial and polyaxial suspended germanium bridges in terms of mechanical stress and thermal management towards a CMOS compatible light source

Daniel Burt,[1] Jofferson Gonzales,[2] Abdelrahman Al-Attili,[3] Harvey Rutt,[1] Ali Z Khokar,[4] Katsuya Oda,[5] Frederic Gardes[4] and Shinichi Saito[1*]

[1] *Sustainable Electronic Technologies, Electronics and Computer Science, University of Southampton, University Road, Southampton, SO17 1BJ, UK*
[2] *Robinson Research Institute, Victoria University of Wellington 69 Gracefield Road, Gracefield, Lower Hutt, Wellington, New Zealand*
[3] *Electrical Engineering Department, School of Engineering Technology, Al Hussein Technical University, 11831, Amman, Jordan*
[4] *Optoelectronics Research Centre, University of Southampton, University Road, Southampton SO17 1BJ, UK*
[5] *Research & Development Group, Hitachi, Ltd., 1-280 Higashi-Koigakubo, Kokubunji, Tokyo 185-8601, Japan*
[*] *ss1a11@ecs.soton.ac.uk*

Abstract: Germanium (Ge) is a promising candidate for a CMOS compatible laser diode. This is due to its compatibility with Silicon (Si) and its ability to be converted into a direct band gap material by applying tensile strain. In particular uniaxial suspended Ge bridges have been extensively explored due to their ability to introduce high tensile strain. There have been two recent demonstrations of low-temperature optically-pumped lasing in these bridges but no room temperature operation accredit to insufficient strain and poor thermal management. In this paper we compare uniaxial bridges with polyaxial bridges in terms of mechanical stress and thermal management using Finite Element Modelling (FEM). The stress simulations reveal that polyaxial bridges suffer from extremely large corner stresses which prevent larger strain from being introduced compared with uniaxial bridges. Thermal simulations however reveal that they are much less thermally sensitive than uniaxial bridges which may indicate lower optical losses. Bridges were fabricated and Raman spectroscopy was used to validate the results of the simulations. We postulate that polyaxial bridges could offer many advantages over their uniaxial counterparts as potential laser devices

1. Introduction

Silicon (Si) photonics potentially offers an elegant solution to the interconnect bottleneck by replacing metallic interconnects with optical equivalents [1]. However, an on-chip Complementary Metal Oxide Semiconductor (CMOS) compatible light source remains the crucial missing component. Si is a poor candidate for an on-chip light source due to its indirect band gap nature which results in inefficient photon emission via phonon assisted recombination [2]. Germanium (Ge) is an exciting candidate for a Si compatible light source and is often referred to as a pseudo-direct band gap material as the energy difference between the direct and indirect valley is relatively small (< 140 meV). Ge can be converted into a direct band gap material by two methods. The first method is tensile strain engineering, the second method is n-type doping to fill the indirect L-valley thus enhancing the probability of injected carriers to populate the direct valley [3, 4].

Tin (Sn) alloying has also been explored. Despite many successful lasing demonstrations in GeSn [5–9] the reported thresholds have been extremely high (between 600-1000 kW cm^{-2}) and far beyond practical use. Furthermore room temperature operation has not yet been achieved with Sn alloying with the highest operating temperature reported being 230 K [9].

A proof of concept optically-pumped Ge laser was demonstrated by Liu *et al* [10] with 0.24% biaxial strain and 1 x 10^{19} cm^{-3} n-type doping resulting in a threshold of 35 kW cm^{-2}. This was followed by a demonstration of an electrically pumped laser diode [11] with 0.25% biaxial strain and 4 x 10^{19} cm^{-3} n-type doping with a threshold of 280 kA cm^{-2}. To reduce the threshold to a practically useful level the amount of strain and n-type doping must be optimized. Ge was thought to be converted into a direct bandgap material at around 1.7% biaxial strain and 4.6% uniaxial strain [12], however more recent experimental and theoretical studies have provided evidence suggesting these values are higher at around 6.0% uniaxial and 2% biaxial strain increasing the challenge of practically achieving optimum strain [13, 14]. One study utilizing tight binding calculations suggested that the optimum configurations for reducing threshold in Ge laser favoured high tensile strain (around 2.5% biaxial strain) with lower n-type doping (around 1 x 10^{19} cm^{-3}) [15].

Many intuitive approaches were adopted to experimentally achieve the high tensile strain required to achieve a practically useful threshold. The two main approaches were: external stressors and suspended bridges. The most common method of using external stressors involves covering the Ge with a material possessing an intrinsic compressive stress, which will subsequently expand upon patterning imparting tensile strain into the Ge. Most research has focused on utilizing Silicon Nitride (Si_3N_4) as the stressor material [16–18]. Silicon Dioxide (SiO_2) has also been utilized as the stressor layer [19–21] however the amount of strain achieved was lower. Suspended bridges were utilized to locally amplify the initial epitaxial tensile strain found in Ge within a bridge using uniaxial [22–25] and polyaxial geometries [15, 26, 27]. These methods also imparted high strain with up to 4.9% uniaxial [24, 28, 29] and 1.9% biaxial [26] strain values respectively.

Despite the higher strain values achieved, reproducing the initial lasing demonstration was difficult, furthermore higher strain values are needed to reach the lowest achievable threshold. There have been two recent demonstrations of optically pumped lasing at low temperature. Elbaz *et al* [18], combined a microdisk optical resonator with a Si_3N_4 stressor having improved thermal management via a metallic pedestal to conduct the heat. Despite the high biaxial strain value of 1.7%, lasing was only observed at 15 K with a threshold of 18 kW cm^{-2}. Bao *et al* [25] used a suspended Ge bridge in a uniaxial nano-wire configuration with 1.6% uniaxial strain, which was subsequently adhered to the underlying SiO_2 via a stiction process to allow transverse thermal conduction. This resulted in a low threshold value of 3 kW cm^{-2} at an operating temperature of 83 K. Both of these recent lasing demonstrations were accredited to improved thermal management which reduced the optical losses, however despite these achievements, efficient room temperature operation has not yet been realized. Even more recently another demonstration of lasing in uniaxial suspended bridges at low temperatures under pulsed optical pumping was reported [30]. The lower temperature measurements and the excellent detailed analysis showed that even at 5.9% strain (achieved by cooling the bridge to lower temperatures the strain value was around 3.0% at room temperature), Ge was still an indirect bandgap material. Only low temperature operation could allow for lasing which inhibits scattering from the direct to indirect valley. It is suggested that higher strain values, that go further than just achieving direct band gap configuration, are required for efficient room temperature (beyond 6.0% for uniaxial and 2.0% for biaxial). Furthermore excellent thermal management will be required to minimize optical losses and achieve room temperature operation. In the case of suspended bridges, polyaxial bridges have been overlooked due to lower achievable strain values. However considering that theoretically 3 times less strain is required to achieve a direct band gap configuration for biaxial strain combined

with better thermal dissipation due to more lateral thermal dissipation, we postulate that polyaxial bridges could offer distinct advantages over uniaxial bridges moving towards higher operation temperatures and steady state operation.

In this paper we study and compare uniaxial and polyaxial suspended Ge bridges along with their respective geometric parameters in terms of mechanical stress and thermal management to understand which configurations could potentially be better for lasing. Finite Element Modelling (FEM) was used to study the influence of various design parameters on the thermal management and mechanical stress. Uniaxial and polyaxial bridges were successfully fabricated on a Ge on SOI (Silicon On Insulator) platform to provide experimental verification of the simulation data. This is done in the form of device survival analysis and Raman spectroscopy. The advantages and disadvantages of using uniaxial or polyaxial bridges will be then discussed in detail.

2. Bridge designs

Figure 1 provides a top view of the uniaxial and polyaxial bridge designs used in this study. The blue regions show the Ge whereas the black regions show the patterned etching windows. In the etching windows, material is removed by dry etching to expose the sacrificial layer underneath. This is followed by an etchant entering these windows and selectively etching the sacrificial layer under etching the Ge resulting in suspension. The maximum distance for the etchant to undercut the Ge was fixed at 10.0 μm in this study as shown in Fig. 1(a). The basic principle of tensile strain engineering in suspended bridges relies on reorganizing the initial tensile biaxial strain of 0.2% introduced during the epitaxial growth of Ge on Si (caused by a mismatch in the Thermal Expansion Coefficients (TECs)) [31]. The larger regions (the pads) compress resulting in the smaller active region being pulled. The geometry of the etching windows is extremely important as it determines the nature (uniaxial/biaxial), magnitude and the distribution of the tensile strain within the bridge.

The design for the uniaxial bridges used in this study is shown in Fig. 1(a). There are four important parameters which are: bridge height, bridge width, filet ratio and pad length. The values of bridge height used in this study were 0.75 μm, 1.5 μm, 2.25 μm and 3.0 μm. The values of bridge width used in this study were 2.5 μm, 5.0 μm, 7.5 μm and 10.0 μm. Filet ratio is a ratio which defines the radius at the edges of the bridge by multiplying this ratio by bridge width, the value was fixed in this study to be 0.25. The pad length used in this study was 30.0 μm.

The design for the polyaxial bridges used in this study is shown in Fig. 1(b). Etch window thickness defines the size of the etch windows and is fixed at 0.3 μm in this study. There are three important parameters which are varied: bridge diameter, the number of arms and the pad length. The values of bridge diameter chosen for this study were 3.0 μm, 4.0 μm, 5.0 μm and 6.0 μm. In this study the number of arms studied was 4, 8, 12, 16 and 20. Pad length is kept at the same value as the uniaxial bridges to allow for a direct comparison.

3. Simulations

In this section Finite Element Modelling (FEM) method was employed using the software package COMSOL Multiphysics 5.3a to study and compare the mechanical stress and thermal sensitivity of uniaxial and polyaxial bridges.

3.1. Stress simulations

A common issue in mechanical design is stress concentration in which stress concentrates at specific points. Usually stress concentration occurs around air holes, this occurs in suspended bridges due to the etch windows. This stress concentration in the suspended bridges can result in mechanical failure, usually in the form of cracking. Stress concentration is is more severe for sharp corners and less severe for curves (and larger radius holes), this is why good suspended

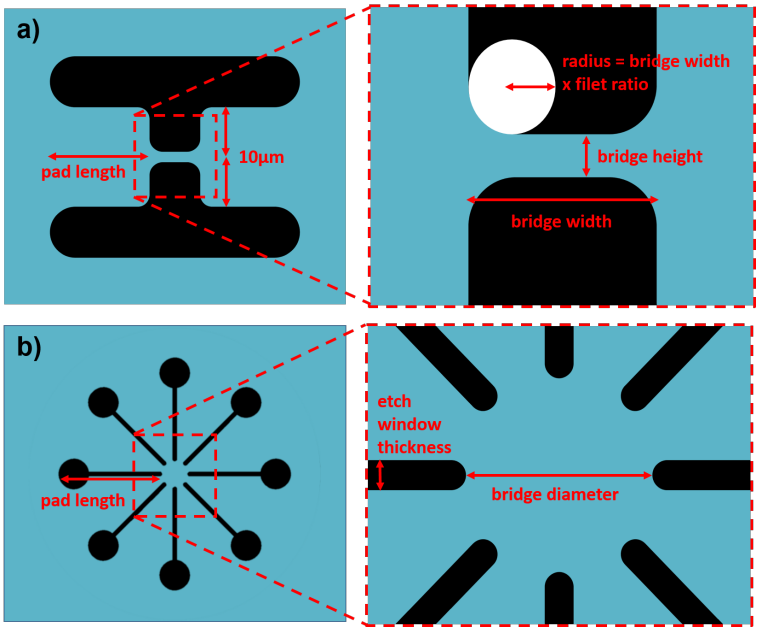

Fig. 1. Exemplar uniaxial and polyaxial bridge designs. (a) Uniaxial design showing the pad length. The central region is shown under zoom and the parameters bridge height, bridge width and filet ratio are defined. The fixed under etch distance of 10.0 μm is also shown. (b) Polyaxial design with 8 arms. The central region is shown and the parameters etch window thickness and bridge diameter are shown.

bridge designs employ curved etch windows. In this section we use the 'Structural Mechanics' module to study corner stresses in uniaxial and polyaxial bridges. A 2D model was created with the bridge geometries. A fixed boundary was applied along the undercut boundary (i.e. where the suspension ends) assuming a 10 μm maximum under etch distance. The initial tensile strain in the system (from the epitaxial growth of Ge on to Si) was set to be 0.2%. The Von Mises stress was plotted for each bridge, this stress was chosen as it factors in the shear components of the stress at which mechanical failure occurs at lower values, compared to equivalent pure symmetric stresses due to a higher distortion of the Ge crystal. The bridge will undergo mechanical failure when the Von Mises stress anywhere in the bridge exceeds a critical value, this value depends on the material quality of the Ge. The central part of the bridge is designed to possess pure uniaxial / biaxial stress (and therefore strain) useful for potential devices. An important ratio is defined between the maximum Von Mises stress in the system (which results from the stress concentration around the etch windows) and the stress in the central region of the bridge. This ratio is labelled the Von Mises Ratio (VMR). The VMR is extremely important as it provides an idea of how much strain can be achieved in the central region of the bridge before mechanical failure occurs due to the maximum Von Mises stress in the bridge exceeding the critical value, therefore lower VMR values are more favourable.

The VMR values were plotted as a function of the relevant geometric parameters for each bridge. This is shown for the uniaxial bridges in Fig. 2(a) and for the polyaxial bridges in Fig. 2(b). Polyaxial bridges have higher VMR values reaching a maximum value of 11.3 compared with the uniaxial bridges which reach a maximum value of of 3.4. The reason that polyaxial bridges posses larger VMR values is due to the presence of shear stresses (assymetric x and y components) at the stress concentrations which results in larger Von Mises stress. This explains

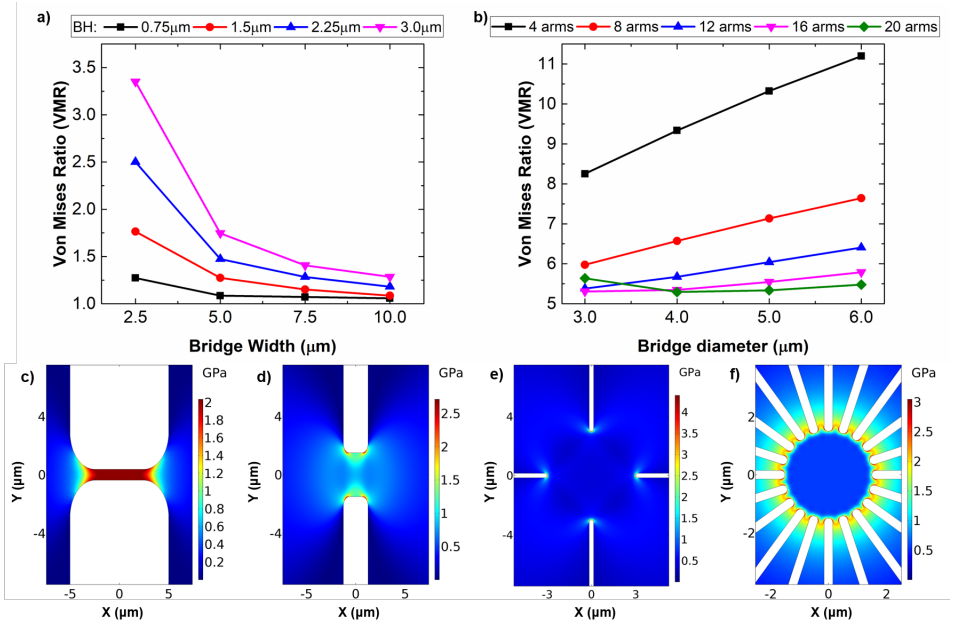

Fig. 2. Results from the stress simulations. **(a)** The influence of bridge width at different bridge heights on the VMR for uniaxial bridges. **(b)** The influence of bridge diameter at different numbers of arms on the VMR for polyaxial bridges. **(c)** Von Mises stress distribution of a uniaxial bridge with a bridge width of 10.0 μm and a bridge height of 0.75 μm. **(d)** Von Mises stress distribution of a uniaxial bridge with a bridge width of 2.5 μm and a bridge height of 3.0 μm. **(e)** Von Mises stress distribution of a polyaxial bridge with a bridge diameter of 6.0 μm and 4 arms. **(f)** Von Mises stress distribution of a polyaxial bridge with a bridge diameter of 3.0 μm and 20 arms.

why much lower strain values are achieved in polyaxial bridges.

Figure 2(a) shows the VMR for the uniaxial bridges as a function of bridge width for various values of bridge height. As bridge width increases the VMR drops and saturates at a value of 6.5 μm. As bridge height decreases the VMR also decreases and at a bridge height of 0.75 μm approaches unity. The Von Mises stress distributions for the two extreme geometries are shown in Fig. 2(c) and Fig. 2(d). In Fig. 2(c). the bridge height is 0.75 μm and the bridge width is 10 μm corresponding to a VMR of 1.05. In Fig. 2(d) the bridge height is 3.0 μm and the bridge width is 2.5 μm corresponding to a VMR of 3.5. Smaller bridge widths and larger bridge heights result in corners with smaller radii (i.e. are more sharp) resulting in greater stress concentration and therefore a higher VMR, this can be visualised in Fig. 2(d). As the bridge height is decreased and the bridge width increased these corner radii are increased therefore reducing the stress concentration, as seen in Fig. 2(c), resulting in a lower VMR. This suggests that the highest strain values should be achieved with lower bridge heights and larger bridge widths.

Figure 2(b) shows the VMR in polyaxial bridges as a function of bridge diameter and for various numbers of arms. Stress is inversely proportional to volume and the force is constant due to the fixed pad length used in this study. As the bridge diameter increases the stress therefore decreases, however the stress concentration does not scale proportionally resulting in a net increase in the VMR. As the number of arms increases the VMR decreases with 4 armed structures possessing extremely high VMR values (>8) as shown in Fig. 2(e). The lowest values for the VMR occurs for bridges with 20 arms. The reason for this is the stress is concentrated

over more points resulting in a lower stress concentration at each point and an overall lower VMR. However if the number of arms is to high and/or the bridge diameter is too small, the etch windows become too close in proximity and high stress builds between them increasing the VMR. This explains why for 20 arms the 3.0 μm bridge diameter has a higher VMR for the 3.5 μm diameter, as visualized in Fig. 3(f). It should be noted that if a large etch window was used for lower arm numbers the VMR would drop to a value comparable to the higher arm numbers, as the stress would be concentrated over a larger radius. However a larger number of arms are more favourable as they introduce more homogeneous strain [32].

3.2. Thermal simulations

For the thermal simulations the Heat Transfer In Solids module was used in conjunction with a 3D geometry. The thickness of the Ge layer was fixed at 200 nm with an air gap underneath to simulate the suspension. The laser beam spot was defined in the center of each bridge. For all simulations, the pump wavelength was fixed at 532 nm and the spot diameter at 0.75 μm so the beam spot fit within all the designs allowing for a fair comparison. To accurately model the heating under optical pumping, the optical power was first calculated. The Fresnel equations were first used to calculate the reflectance and transmission of the incident light into the Ge layer, the beam profile was modelled as a 2D Gaussian function at the surface therefore accounting for lateral non-uniformity. The transverse non-uniformity was considered by implementing the Beer-Lambert law. The optical power distribution was subsequently used as a heat source under the assumption that all the optical power was converted to heat. The bottom of the silicon substrate underneath the air gap was set to be 20 ^{o}C as a fixed boundary condition.

The temperature increase (i.e. compared to an ambient of 20 degrees Celsius) at the central point of the bridges was plotted as a function of the relevant geometric parameters to give an indication of the thermal sensitivity of the bridge (i.e. more thermally sensitive bridges result in higher temperature rises at equivalent pump power). This is shown for the uniaxial bridges in Fig. 3(a) for different bridge widths and bridge heights and for the polyaxial bridges in Fig. 3(b) for different bridge diameters and numbers of arms.

Due to the air gap underneath the bridges inhibiting efficient transverse thermal dissipation, the suspended bridges rely on lateral thermal dissipation from the central bridge region to the pads. The lateral thermal dissipation in turn relies on solid (i.e. Ge) thermal conduction paths and therefore will be inhibited by an increased area of the etchant window (i.e. air gaps) resulting in higher temperatures.

Figure 3(a) shows that for the uniaxial bridges, larger bridge widths and smaller bridge heights cause more heating and vice versa. The temperature profiles for the two extreme cases are shown in Fig. 3(c) and 3(d). In Fig. 3(c) the bridge height is 3.0 μm and bridge width is 2.5 μm which corresponds to the smallest temperature rise of 125 ^{o}C. At larger bridge widths the heat from the center of the bridge has a further distance to travel to dissipate at the pads. In Fig. 3(d) the bridge height is 0.75 μm and bridge width is 10.0 μm which corresponds to the highest temperature rise of 375 ^{o}C. At smaller bridge heights lateral thermal dissipation is reduced resulting in more heating, this results in severe heating at the lowest bridge height value of 0.75 μm.

Figure 3(b) shows that for the polyaxial bridges, smaller bridge diameters and a higher number of arms result in more heating and vice versa. The temperature profiles for the two extreme cases of the geometry are shown in Fig. 3(e) and 3(f). In Fig. 3(e) the inner diameter is 6.0 μm and the number of arms is 4 corresponding to the lowest temperature rise of 83 ^{o}C. In Fig. 2(f) the inner diameter is 3.0 μm and the number of arms is 20 corresponding to the highest temperature rise of 93 ^{o}C. At smaller bridge diameters and higher number of arms the distance between etch windows is reduced restricting thermal dissipation from the bridge into the pads.

It should be noted that the range of temperature increase is larger for the uniaxial bridges (125 ^{o}C to 375 ^{o}C) compared with polyaxial bridges (83 ^{o}C to 94 ^{o}C) meaning that the heating in

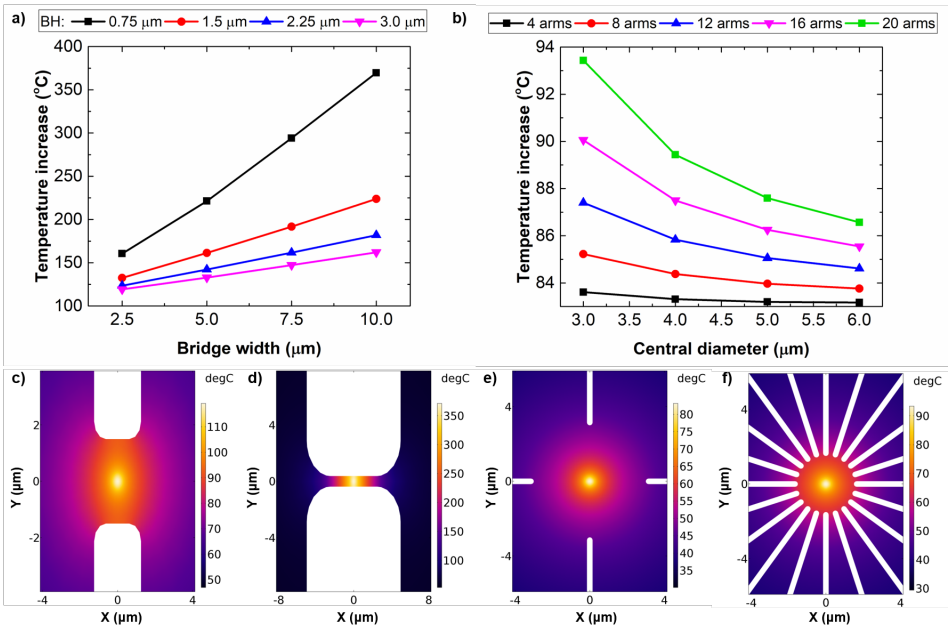

Fig. 3. Results from the thermal simulations. **(a)** The influence of bridge width at different bridge heights on the central temperature increase for uniaxial bridges. **(b)** The influence of bridge diameter at different numbers of arms on the central temperature increase for polyaxial bridges. **(c)** The temperature distribution of a uniaxial bridge with a bridge width of 2.5 μm and a bridge height of 3.0 μm under 1 mW pump power. **(d)** The temperature distribution of a uniaxial bridge with a bridge width of 10.0 μm and a bridge height of 0.75 μm under 1mW pump power. **(e)** The temperature distribution of a polyaxial bridge with a bridge diameter of 6.0 μm and 4 arms under 1 mW pump power. **(f)** The temperature distribution of a polyaxial bridge with a bridge diameter of 3.0 μm and 20 arms under 1 mW pump power.

uniaxial bridges are more sensitive to design parameters than the polyaxial bridges. This can be explained by the much larger variation in the air gap surrounding the central region with the uniaxial geometric parameters compared with the polyaxial geometric parameters which can be visualized in Figs. 2(c)-2(f).

4. Experimental validation

4.1. Fabrication process

Figure 4 shows the main fabrication steps to produce the suspended bridges on two 1 cm by 1 cm chips taken from a Ge on SOI wafer. The chips were first cleaned to remove any organic contaminants from the surface using N-Methyl-2-pyrrolidone (NMP) under sonication followed by rinsing with Iso-Propyl Alcohol (IPA). This was followed by the spin-coating of the electronic resist ZEP520A. Electron beam lithography (EBL) was then used to define the etching windows (and therefore the bridges). After development the chips underwent Inductively Coupled Plasma (ICP) dry etching using CHF_3 and SF_6 chemistry removing the Ge and SOI and exposing the Buried Oxide (BOX) thus forming the etch windows. The remaining resist was then removed using elevated temperature NMP followed by IPA. Both chips underwent liquid HydroFluoric (HF) acid etching to remove the sacrificial BOX underneath the bridges and suspend the bridges.

Due to the small Ge layer thickness of 200 nm and also the small BOX thickness of 145 nm stiction was a concern. A simple tuning of the gap underneath the Ge was developed to prevent stiction, one chip was placed into TetraMethylAmmonium Hydroxide (TMAH) after the HF suspension and rinsing with De-Ionised (DI) water with no drying step in between to tune etching of the Si handle layer increasing the gap underneath the bridges. After all the etching steps both chips were rinsed in DI water and dried using a nitrogen gun. This tuning resulted in a gap of around 10 μm underneath the Ge and used to reduce capillary forces during the subsequent drying step to prevent stiction. The structures that underwent the additional TMAH etching to make the gap underneath the bridge larger will be referred to as "tuned". Conversely the structures that just underwent HF etching will be referred to as "not tuned".

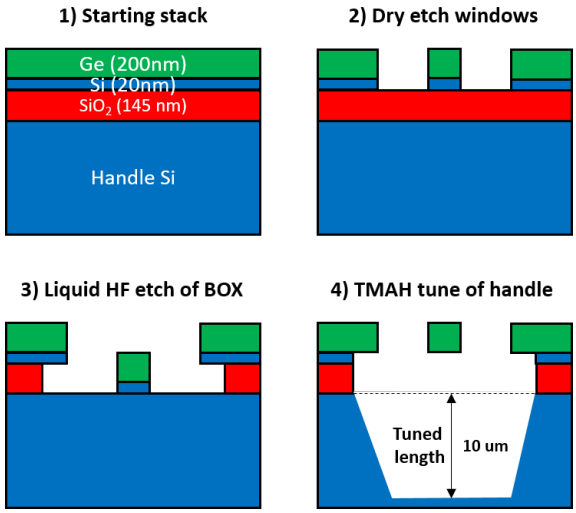

Fig. 4. A schematic showing the starting wafer stack of the Ge on SOI platform and the main stages of fabrication.

4.2. Optical micro-graphs and yield analysis

Figure 5(a) shows exemplar optical micro-graphs of the successfully fabricated Ge bridges with the uniaxial bridges on the top row and polyaxial bridges on the bottom row. Furthermore bridges with identical designs which were not tuned are shown on the left hand side with bridges that were tuned shown on the right hand side. The etchant windows in the uniaxial and polyaxial bridges can be seen to be visibly darker in the tuned bridges indicating a much deeper gap suggesting the tuning process was successful.

Figure 5(b) shows the percentage survival rate of the uniaxial and polyaxial bridges (i.e. the percentage of bridges that had not undergone mechanical failure) for both the tuned and not tuned bridges. The uniaxial bridges had a much higher survival rate compared with the polyaxial designs. The polyaxial bridges that were not tuned have a survival rate of 8.1% whereas the uniaxial bridges have a much higher 45.0% survival rate. The polyaxial bridges that were tuned had a survival rate of 15.0% whereas the uniaxial bridges that were tuned again had a much larger 75.0% survival rate. This agrees with the results of the stress simulation as the polyaxial bridges have a much lower survival rate due to higher corner stresses and thus higher VMR values. The fact that the tuned bridges have a larger survival rate than the bridges that were not tuned, is likely due to the larger capillary forces introduced during drying in the not tuned bridges. The capillary forces act on the fragile highly stressed bridges causing mechanical failure. This reduction of

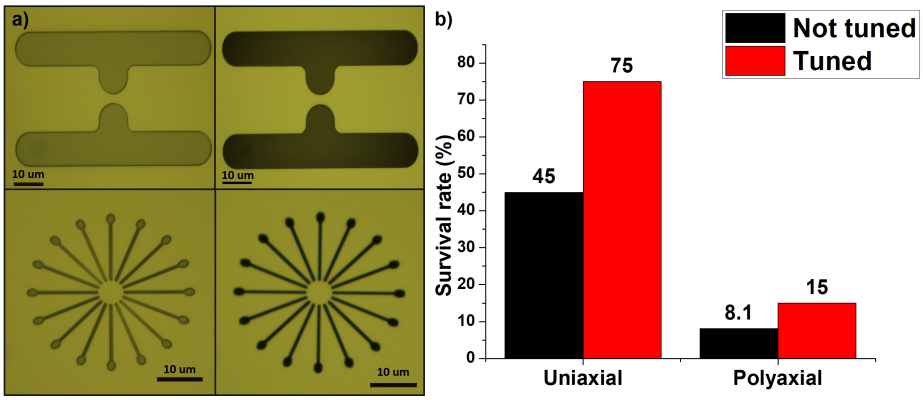

Fig. 5. Surviving devices and bar-graph indicating the survival rate of the devices. **(a)** Surviving uniaxial (top row) and polyaxial (bottom row) for the not tuned (left column) and tuned (right column) bridges. **(b)** Bar graph comparing the survival rate of uniaxial and polyaxial bridges with and without tuning.

bridge survival due to larger capillary forces is supported by the fact that the highest strained structures reported in literature utilized a dry release thus eliminating the need for a drying step and thus drastically reducing the capillary forces [24, 26]. This simple tuning technique can be applied not only to prevent stiction, which was the original goal, but also to improve the yield of bridges and achieve higher strain values. The aim of this study was to focus on fully suspended bridges and not bridges that had undergone stiction to the underlying Si (which would cause optical leakage in actual laser diode devices).

4.3. Raman spectroscopy

Raman spectroscopy was used to validate the results of the stress and thermal simulations. A continuous wave green laser with a wavelength of 514 nm was used to excite the bridges. A 50x objective lens was used to focus the laser spot onto the central area of the bridge resulting in a spot diameter of around 1.0 μm. The signal was collected using the same objective lens and reflected into a high resolution grating of 3000 lines/mm. The exposure time was set to 10 s and the spectra were averaged 12 times for a total measurement time of 120 s per bridge. The Raman spectra were fitted with Lorentzian functions in order to estimate the peak position.

For measuring the strain, an optical power of 46 μW was used after testing the power dependency and showing negligible heating effects (which cause an error in the strain measurement). Shifts in Raman peak position relative to a bulk Ge sample ($\Delta\omega$) were deduced allowing the strain (ϵ) to be calculated using the equation: $\epsilon = \Delta\omega$ x C. Where C is a proportionality factor reported in literature to be 390 cm^{-1} [16] for biaxial strain and 152 cm^{-1} for uniaxial strain [22].

Figure 6(a) shows the Raman spectra of the polyaxial and uniaxial bridges with the highest strain. The uniaxial bridge with the highest uniaxial strain value of 2.55% had a bridge height of 0.75 μm and a bridge width of 7.5 μm. This coincides with the results of the simulations in which the VMR was lowest for smaller bridge heights and widths. The polyaxial bridge with the highest biaxial strain value of 0.75% had a bridge diameter of 3.0 μm and 20 arms. This also agrees with the stress analysis of the polyaxial bridges which showed that lower bridge diameters and a higher numbers of arms possessed a lower VMR.

For validating the thermal simulations, two exemplar bridges were compared with the simulation results: one polyaxial and one uniaxial. The uniaxial bridge had a bridge width of 7.5 μm and a bridge height of 10.0 μm. The polyaxial bridge had a bridge diameter of 3.0 μm and 20 arms.

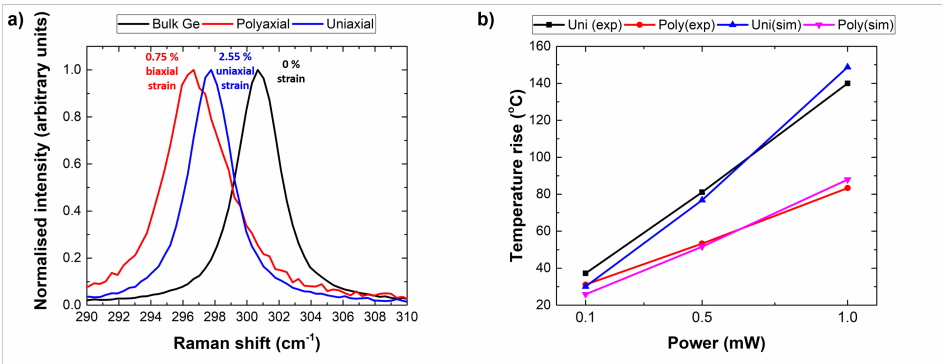

Fig. 6. The results of the Raman spectroscopy. **(a)** Raman spectra of the bulk Ge sample and the bridges with the highest uniaxial and biaxial strain. **(b)** Temperature rise from finite element modelling and Raman thermometry for an exemplar uniaxial and polyaxial bridge to verify simulation results.

The Raman spectra were recorded at 0.1, 0.5 and 1.0 mW of power and the peak positions were extracted with Lorentzian fitting. The peak positions were plotted as a function of power and a linear fit was performed and extrapolated to the y-axis to give the peak position under zero power and remove the effect of strain. The difference of the Raman positions at each power with this zero power position were then calculated and the temperature rise was calculated assuming a linear relationship and dividing the shift by the constant 0.0160 cm^{-1} [33]. The temperature increase was plotted as a function of power and the results of simulations under identical conditions were also plotted in Fig. 6(b). As shown in Fig. 6(b) the simulation data is in excellent agreement with the experimental data.

5. Discussion

For uniaxial bridges there is a severe trade off between achieving higher strain and minimizing heating. Smaller bridge heights and larger bridge widths favour higher strain. This is supported by literature, with the highest uniaxial strains reported possessing bridge heights in the range of 200.0 nm and bridge widths of 4.5 μm [24, 28, 29]. However smaller bridge heights and larger bridge widths result in higher temperatures meaning the bridge designs that allow for the highest strain are also extremely thermally sensitive.

For polyaxial bridges there is also a trade off between achieving higher strain and minimizing thermal sensitivity. Larger numbers of arms and smaller bridge diameters result in lower shear stresses and thus a higher achievable strain (and also improved strain homogeneity), but this results in higher thermal sensitivity and vice versa. However the dependence of thermal sensitivity on geometric parameters in polyaxial bridges is small when compared to the uniaxial bridges, as shown in the simulation section of this study.

Polyaxial bridges have been less extensively explored compared to uniaxial bridges, mostly due to the lower amount of strain achieved. However the results from this study combined with recent reports in literature suggest that polyaxial bridges are actually more favourable to their uniaxial counterparts. The highest achieved uniaxial strain in uniaxial bridges was 4.9% whereas the highest biaxial strain in polyaxial bridges was 1.9%. But recent theoretical and experimental evidence shows that, the amount of strain required to convert Ge into a direct bandgap material is three times larger for uniaxial strain (6.0%) compared to biaxial strain (2.0%) [13, 14]. Therefore polyaxial bridges not only possess superior thermal management, but they are also closer to achieving the direct bandgap configuration in Ge.

Furthermore to achieve the highest strain in uniaxial bridges, the bridge width must be very small. In literature the highest values of 4.9% were only achieved in extremely thin nanowires with wire heights of 200 nm. However this will result in extreme heating, causing unacceptable optical losses. Furthermore an optical mode is extremely difficult to confine in such a narrow wire [24].

With uniaxial bridges, as the VMR has almost approached unity by careful design, to further increase the strain the material quality must be improved (i.e. dislocations reduced) to prevent fracturing. On the other hand the VMR in polyaxial designs is still larger than unity. This offers an opportunity to introduce higher biaxial strain by improving the design to reduce corner stress. In other words the maximum strain in uniaxial bridges is inherently limited by material quality whereas polyaxial bridges have the potential to achieve higher strain and therefore optical gain by improved designs.

One major issue preventing the achievement of room temperature operation is absorption due to intra-band transitions. Gupta *et al* showed by modelling the Inter Valence Band Absorption (IVBA) under the influence of strain, that for certain uniaxial strain values, there was a resonance between the gain and loss mechanisms. It was theoretically predicted that net gain was achieved between 4% to 5% uniaxial strain. This has an important implication that strain must be optimised, and not just increased indefinitely, to achieve room temperature lasing. However the cross over from direct bandgap in the study by Gupta *et al* is underestimated at 4.6% (1.4% underestimation) which means the range of strain value at which the optimum gain is achieved is also underestimated. The largest uniaxial strain achieved in literature is 4.9% and therefore is still not optimum. One must also considering the limitations of introducing more uniaxial strain. Therefore polyaxial bridges introducing biaxial strain offer a more effective way to achieve these ideal strain value for minimising absorption losses and maximising optical gain.

Finally it should be noted that the temperature rise for bridge suspended in air is still too large for practical device operation. Stiction to the underlying Si would drastically improve thermal management due to the high thermal conductivity of Si (i.e. in 'not tuned' structures). However if the Ge undergoes stiction to the Si the refractive index contrast is low introducing large optical losses and therefore is avoided. Previous studies in suspended bridges have utilised stiction to SiO_2 to maintain a large refractive index contrast whilst providing transverse thermal conduction paths for the bridges [15, 23, 34]. However SiO_2 still has a relatively low thermal conductivity when compared to Ge or Si (around 2 orders of magnitude lower). Future work can involve combining optimised polyaxial bridges to provide excellent lateral thermal heat dissipation with the transverse thermal heat dissipation into the SiO_2. This will not only drastically improve the thermal management to an acceptable level in the bridges, but by using higher quality GOI will allow for higher biaxial strain values to be achieved.

6. Conclusions

We have investigated uniaxial and polyaxial bridges in terms of mechanical stress and thermal sensitivity. FEM showed that the polyaxial bridges suffered from large corner stresses thus inhibiting large strain to be achieved. On the other hand uniaxial bridges can be designed to have negligible corner stresses allowing higher strain to be achieved. However FEM also revealed that uniaxial bridges were much more thermally sensitive under optical pumping which will cause detrimental optical losses in potential laser devices. To provide verification of the simulation results, suspended bridges were fabricated and underwent Raman spectroscopy which showed excellent agreement with the simulations. With the lower thermal sensitivity and less strain required for a direct band gap configuration, we argue that despite being overlooked compared with uniaxial bridges, polyaxial bridges have great potential for lasing.

Funding

This work is supported by EPSRC Manufacturing Fellowship (EP/M008975/1), EU FP7 Marie-Curie Carrier-Integration grant (PCIG13-GA-2013-61811), and EPSRC Institutional Sponsorship Research Collaboration. The data from the paper can be obtained from the University of Southampton e-Print research repository: https://doi.org/10.5258/SOTON/D1048

Acknowledgments

We would like to thank Professor Robert Kelsall and Dr Ekaterina Orlova from the University of Leeds for their thoughtful discussions. We would also like to thank Moise Sötto for his thoughtful advice.

References

1. G. Reed, *Silicon Photonics: An Introduction* (John Wiley and Sons, Ltd, 2004).
2. F. Herman, "The electronic energy band structure of silicon and germanium," Proc. IRE **43**, 1703–1732 (1955).
3. J. Liu, X. Sun, D. Pan, X. Wang, L. C. Kimerling, T. L. Koch, and J. Michel, "Tensile-strained, n-type ge as a gain medium for monolithic laser integration on si," Opt. Express **15**, 11272–11277 (2007).
4. J. Liu, X. Sun, L. C. Kimerling, and J. Michel, "Direct-gap optical gain of ge on si at room temperature," Opt. Lett. **34**, 1738–1740 (2009).
5. S. Wirths, R. Geiger, N. von den Driesch, G. Mussler, T. Stoica, S. Mantl, Z. Ikonic, M. Luysberg, S. Chiussi, J. M. Hartmann, H. Sigg, J. Faist, D. Buca, and D. Grützmacher, "Lasing in direct-bandgap gesn alloy grown on si," Nat. Photonics **9**, 88 (2015).
6. D. Stange, S. Wirths, R. Geiger, C. Schulte-Braucks, B. Marzban, N. von den Driesch, G. Mussler, T. Zabel, T. Stoica, J.-M. Hartmann, S. Mantl, Z. Ikonic, D. Grutzmacher, H. Sigg, J. Witzens, and D. Buca, "Optically pumped gesn microdisk lasers on si," ACS Photonics **3**, 1279–1285 (2016).
7. V. Reboud, A. Gassenq, N. Pauc, J. Aubin, L. Milord, Q. M. Thai, M. Bertrand, K. Guilloy, D. Rouchon, J. Rothman, T. Zabel, F. Armand Pilon, H. Sigg, A. Chelnokov, J. M. Hartmann, and V. Calvo, "Optically pumped gesn micro-disks with 16% sn lasing at 3.1 μm up to 180k," Appl. Phys. Lett. **111**, 092101 (2017).
8. W. Dou, Y. Zhou, J. Margetis, S. A. Ghetmiri, S. Al-Kabi, W. Du, J. Liu, G. Sun, R. A. Soref, J. Tolle, B. Li, M. Mortazavi, and S.-Q. Yu, "Optically pumped lasing at 3μm from compositionally graded gesn with tin up to 22.3%," Opt. Lett. **43**, 4558–4561 (2018).
9. Q. M. Thai, N. Pauc, J. Aubin, M. Bertrand, J. Chrétien, V. Delaye, A. Chelnokov, J.-M. Hartmann, V. Reboud, and V. Calvo, "Gesn heterostructure micro-disk laser operating at 230 k," Opt. Express **26**, 32500–32508 (2018).
10. J. Liu, X. Sun, R. Camacho-Aguilera, L. C. Kimerling, and J. Michel, "Ge-on-si laser operating at room temperature," Opt. Lett. **35**, 679–681 (2010).
11. R. E. Camacho-Aguilera, Y. Cai, N. Patel, J. T. Bessette, M. Romagnoli, L. C. Kimerling, and J. Michel, "An electrically pumped germanium laser," Opt. Express **20**, 11316–11320 (2012).
12. O. Aldaghri, Z. Ikonic, and R. W. Kelsall, "Optimum strain configurations for carrier injection in near infrared ge lasers," J. Appl. Phys. **111**, 053106 (2012).
13. J. M. Escalante, "Non-linear behavior of germanium electronic band structure under high strain," Comput. Mater. Sci. **152**, 223 – 227 (2018).
14. K. Guilloy, N. Pauc, A. Gassenq, Y.-M. Niquet, J.-M. Escalante, I. Duchemin, S. Tardif, G. Osvaldo Dias, D. Rouchon, J. Widiez, J.-M. Hartmann, R. Geiger, T. Zabel, H. Sigg, J. Faist, A. Chelnokov, V. Reboud, and V. Calvo, "Germanium under high tensile stress: Nonlinear dependence of direct band gap vs strain," ACS Photonics **3**, 1907–1911 (2016).
15. D. S. Sukhdeo, S. Gupta, K. C. Saraswat, B. R. Dutt, and D. Nam, "Ultimate limits of biaxial tensile strain and n-type doping for realizing an efficient low-threshold ge laser," Jpn. J. Appl. Phys. **55**, 024301 (2016).
16. G. Capellini, G. Kozlowski, Y. Yamamoto, M. Lisker, C. Wenger, G. Niu, P. Zaumseil, B. Tillack, A. Ghrib, M. de Kersauson, M. El Kurdi, P. Boucaud, and T. Schroeder, "Strain analysis in sin/ge microstructures obtained via si-complementary metal oxide semiconductor compatible approach," J. Appl. Phys. **113**, 013513 (2013).
17. G. Capellini, C. Reich, S. Guha, Y. Yamamoto, M. Lisker, M. Virgilio, A. Ghrib, M. E. Kurdi, P. Boucaud, B. Tillack, and T. Schroeder, "Tensile ge microstructures for lasing fabricated by means of a silicon complementary metal-oxide-semiconductor process," Opt. Express **22**, 399–410 (2014).
18. A. Elbaz, M. El Kurdi, A. Aassime, S. Sauvage, X. Checoury, I. Sagnes, C. Baudot, F. Boeuf, and P. Boucaud, "Germanium microlasers on metallic pedestals," APL Photonics **3**, 106102 (2018).
19. A. Al-Attili, M. Husain, F. Gardes, H. Arimoto, S. Saito, N. Higashitarumizu, Y. Ishikawa, S. Kako, S. Iwamoto, and Y. Arakawa, "Fabrication of ge micro-disks on free-standing sio2 beams for monolithic light emission," in *2015 IEEE 15th International Conference on Nanotechnology (IEEE-NANO),* (2015).
20. A. Z. Al-Attili, S. Kako, M. K. Husain, F. Y. Gardes, S. Iwamoto, Y. Arakawa, and S. Saito, "Tensile strain engineering of germanium micro-disks on free-standing sio 2 beams," Jpn. J. Appl. Phys. **55** (2016).

21. A. Z. Al-Attili, D. Burt, Z. Li, N. Higashitarumizu, F. Y. Gardes, K. Oda, Y. Ishikawa, and S. Saito, "Germanium vertically light-emitting micro-gears generating orbital angular momentum," Opt. Express **26**, 34675–34688 (2018).
22. M.Suess, R.Geiger, R.A.Minamisawa, G.Schiefler, D.Chrastina, R. G Isella, J.Faist, and H.Sigg, "Analysis of enhanced light emission from highly strained germanium microbridges," Nat. Photonics pp. 446–472 (2013).
23. D. Nam, D. S. Sukhdeo, J.-H. Kang, J. Petykiewicz, J. H. Lee, W. S. Jung, J. Vuckovic, M. L. Brongersma, and K. C. Saraswat, "Strain-induced pseudoheterostructure nanowires confining carriers at room temperature with nanoscale-tunable band profiles," Nano Lett. **13**, 3118–3123 (2013).
24. D. S. Sukhdeo, D. Nam, J.-H. Kang, M. L. Brongersma, and K. C. Saraswat, "Direct bandgap germanium-on-silicon inferred from 5.7% uniaxial tensile strain," Photon. Res. **2**, A8–A13 (2014).
25. S. Bao, D. Kim, C. Onwukaeme, S. G. ad Krishna Saraswat, K. H. Lee, Y. Kim, D. Min, Y. Jung, H. Qiu, H. Wang, E. A. Fitzgerald, C. S. Tan, and D. Nam, "Low-threshold optically pumped lasing in highly strained germanium nanowires," Nat. Commun. (2017).
26. A. Gassenq, K. Guilloy, G. Osvaldo Dias, N. Pauc, D. Rouchon, J.-M. Hartmann, J. Widiez, S. Tardif, F. Rieutord, J. Escalante, I. Duchemin, Y.-M. Niquet, R. Geiger, T. Zabel, H. Sigg, J. Faist, A. Chelnokov, V. Reboud, and V. Calvo, "1.9% bi-axial tensile strain in thick germanium suspended membranes fabricated in optical germanium-on-insulator substrates for laser applications," Appl. Phys. Lett. **107**, 191904 (2015).
27. D. Burt, A. Al-Attili, Z. Li, F. Gardès, M. Sotto, N. Higashitarumizu, Y. Ishikawa, K. Oda, O. M. Querin, S. Saito, and R. Kelsall, "Enhanced light emission from improved homogeneity in biaxially suspended germanium membranes from curvature optimization," Opt. Express **25**, 22911–22922 (2017).
28. V. Reboud, A. Gassenq, K. Guilloy, G. O. Dias, J. M. Escalante, S. Tardif, N. Pauc, J. M. Hartmann, J. Widiez, E. Gomez, E. B. Amalric, D. Fowler, D. Rouchon, I. Duchemin, Y. M. Niquet, F. Rieutord, J. Faist, R. Geiger, T. Zabel, E. Marin, H. Sigg, A. Chelnokov, and V. Calvo, "Ultra-high amplified strain on 200 mm optical Germanium-On-Insulator (GeOI) substrates: towards CMOS compatible Ge lasers," in *Silicon Photonics XI,* vol. 9752 G. T. Reed and A. P. Knights, eds., International Society for Optics and Photonics (SPIE, 2016), pp. 73 – 80.
29. V. Reboud, J. Widiez, J. M. Hartmann, G. O. Dias, D. Fowler, A. Chelnokov, A. Gassenq, K. Guilloy, N. Pauc, V. Calvo, R. Geiger, T. Zabel, J. Faist, and H. Sigg, "Structural and optical properties of 200 mm germanium-on-insulator (GeOI) substrates for silicon photonics applications," in *Silicon Photonics X,* vol. 9367 G. T. Reed and M. R. Watts, eds., International Society for Optics and Photonics (SPIE, 2015), pp. 231 – 236.
30. F. T. Armand Pilon, A. Lyasota, Y.-M. Niquet, V. Reboud, V. Calvo, N. Pauc, J. Widiez, C. Bonzon, J. M. Hartmann, A. Chelnokov, J. Faist, and H. Sigg, "Lasing in strained germanium microbridges," Nat. Commun. **10**, 2724 (2019).
31. Y. Ishikawa, K. Wada, D. D. Cannon, J. Liu, H.-C. Luan, and L. C. Kimerling, "Strain-induced band gap shrinkage in ge grown on si substrate," Appl. Phys. Lett. **82**, 2044–2046 (2003).
32. D. S. Sukhdeo, J. Petykiewicz, S. Gupta, D. Kim, S. Woo, Y. Kim, J. Vuckovic, K. C. Saraswat, and D. Nam, "Ge microdisk with lithographically-tunable strain using cmos-compatible process," Opt. Express **23**, 33249–33254 (2015).
33. J. Jaramillo-Fernandez, E. Chavez-Angel, and C. M. Sotomayor-Torres, "Raman thermometry analysis: Modelling assumptions revisited," Appl. Therm. Eng. **130**, 1175 – 1181 (2018).
34. J. Petykiewicz, D. Nam, D. S. Sukhdeo, S. Gupta, S. Buckley, A. Y. Piggott, J. Vučković, and K. C. Saraswat, "Direct bandgap light emission from strained germanium nanowires coupled with high-q nanophotonic cavities," Nano Lett. **16**, 2168–2173 (2016). PMID: 26907359.